Photothermally Reconfigurable Colloidal Crystals at a Fluid Interface, a Generic Approach for Optically Tunable Lattice Properties

Jacopo Vialetto, Sergii Rudiuk, Mathieu Morel, Damien Baigl

Photothermally reconfigurable colloidal crystals at a fluid interface, a generic approach for optically tunable lattice properties

Journal:	*Journal of the American Chemical Society*
Manuscript ID	ja-2021-042208.R1
Manuscript Type:	Article
Date Submitted by the Author:	n/a
Complete List of Authors:	Vialetto, Jacopo; ETH Zurich - D-MATL, Department of Materials Rudiuk, Sergii; Ecole Normale Superieure, Department of Chemistry Morel, Mathieu; Ecole Normale Superieure, Department of Chemistry Baigl, Damien; Ecole Normale Superieure, Department of Chemistry

Photothermally reconfigurable colloidal crystals at a fluid interface, a generic approach for optically tunable lattice properties

Jacopo Vialetto,*† Sergii Rudiuk, Mathieu Morel,* and Damien Baigl

PASTEUR, Department of Chemistry, École Normale Supérieure, PSL University, Sorbonne Université, CNRS, 75005 Paris, France.

E-mail: jacopo.vialetto@mat.ethz.ch (JV); mathieu.morel@ens.psl.eu (MM).

† Current address: *Laboratory for Soft Materials and Interfaces, Department of Materials, ETH Zürich, Zürich, Switzerland.*

Abstract

Optically addressable colloidal assembly at fluid interfaces is a highly desired component to generate reconfigurable 2D materials, but has rarely been achieved and only with specific interface engineering. Here we describe a generic method to get optically reconfigurable colloidal crystals at the air/water interface and emphasize a new mechanism to convert light into tunable lattice properties. We use light-absorbing anionic particles adsorbed at the air/water interface in the presence of minute amounts of cationic surfactant, which self-assembled into closely-packed polycrystalline structures by collectively deforming the surrounding interface. Low-intensity irradiation of these colloidal crystals results in unprecedented control of the interparticle spacing (IPS) in a preserved crystalline state while, at a higher intensity, cycles of melting/recrystallization with a controllable transition kinetics can be achieved upon successive on/off stimulations. We show that this photoreversible melting originates from an initial thermocapillary stress, expanding the colloidal assembly against the local confinement, and an increase in particles diffusivity imposing the transition kinetics. With this mechanism, local irradiation leads to highly dynamic patterns, including self-healing or self-fed "living" crystals, while multi-responsive assembly is also achieved by controlling particle organization with both light and magnetic stimuli.

Introduction

Colloidal particles are commonly employed as building blocks for the fabrication of functional materials and devices.[1,2] This relies on the capacity of colloids to self-organize into long-range ordered architectures. Of particular interest is their assembly at fluid interfaces, where the liquid surface acts as a template to direct and control organization in two-dimensional (2D) structures,[3–5] obtaining materials subsequently used, to name a few, as masks for colloidal lithography,[6] liquid mirrors,[7] sensors,[8] or coatings with iridescent colourations[9]. Particle mobility at the liquid interface allows for precise and dynamic control over the assembly processes, which is of remarkable importance to tune on-demand the resulting structures,[10–12] leading to novel stimulus-responsive functionalities but also a better understanding of the collective behaviors at play.

Several strategies have been developed to tune the structural organization of particle assemblies floating on liquid interfaces: for example upon variation of pH or ionic strength of the aqueous subphase,[8,13–15] by adding surface-active molecules,[15–18] or by changing the surface pressure by means of moving barriers.[11,19–21] However, those methods cannot be employed for dynamic control over already organized particles, a concept of exceptional importance for the construction of stimuli-responsive devices. For this purpose, light is an attractive stimulus, offering the possibility to switch on-demand the interactions among colloids in self-assembled structures.[22–25] On solid substrates, light-induced control over 2D structures has been reported for photocatalytic Janus particles with well-defined surface chemistry,[26,27] using light-absorbing particles in a water/lutidine mixture,[28] or by using optical gradient forces.[29,30] At liquid/liquid interfaces, light stimulation has been employed to induce the motion[31–33] and spinning[34] of single particles, or to move particles aggregates.[35] But to our knowledge, dynamic control over crystalline organization has been achieved only recently and using chemically-engineered interfaces (particles and/or surfactants). One example was the controlled colloidal crystallization at an oil/water interface by laser irradiation through a combination of optical trapping and thermophoresis. This led to optically addressable, yet very small, assemblies, and it required specific interaction between DNA-modified particles to achieve reversible transitions.[36,37] A second achievement was the dissipative crystals, reported by our group, formed by anionic particles mixed with a cationic photosensitive surfactant.[38] Based on the out-of-equilibrium adsorption/desorption dynamics of the surfactant isomers at/from the water surface, cycles between disordered (without stimulus) and highly crystalline (under light) colloidal structures of millimeter size were achieved. This approach had however some limitations: it required the addition of a specific photosensitive surfactant and the ordered structures were stable only under constant irradiation. Both cases were thus system-specific and no generic method to control 2D crystallization, and even optically modulate the inter-

particle distance, has been reported so far. Additionally, optical modulation of inter-particle distance in ordered 2D colloidal crystals was never reported.

With the objective to overcome such limitations, we have developed a novel generic principle and achieve a higher spatio-temporal control over the organization of colloids at a fluid interface. We show here that a visible light source of moderate power allows one to tune the structural organization of inherently absorbing particles, without the need of specific engineering of interface chemistry nor complex optical set-up. To ensure a significant response to light, we used commercial particles with iron oxide inclusions. The incident light absorbed by the particles resulted in a local increase in thermal energy, further converted into mechanical energy by means of Marangoni stress and increased diffusivity. This energy conversion allowed us to control quantitatively and reversibly, based on the light intensity used, the interparticle spacing in 2D crystals up to complete disassembly, and to tune the kinetics of melting, and subsequent re-crystallization, of this colloidal system. By structural analysis, single-particle tracking and velocity field mapping, we deciphered the mechanisms governing these transitions. Furthermore, patterned light irradiation allowed to reach interesting dynamic states, such as self-healing crystals where a locally melted zone can be guided and repaired, or "living" colloidal crystals where particles continuously escaped from, and successively re-entered, the ordered assembly. Finally, multiresponsive assemblies were explored by applying both light and magnetic stimulations.

Results and Discussion

Our experimental system is composed of 4.5 μm diameter (D_p) anionic polystyrene particles with homogeneous incorporation of nanometer-sized iron oxide crystallites (Fig. 1a), allowing such particles to absorb visible light. To obtain colloidal crystals at the air/water interface, we used a previously described protocol, the "flipping method".[17,18] The light-absorbing colloids were mixed with an aqueous solution of cationic surfactant dodecyltrimethylammonium bromide (DTAB, concentration C_s = 1 μM) in a 7 mm cylindrical cell. DTAB was added in minute quantity in order to screen the adsorption barrier between anionic particles and the air/water interface, without neutralizing the particle surface charge. The cell was first flipped upside down to let particles reach and adsorb at the air/water interface, prior to be flipped back in its initial position. Due to a contact angle of about 80° between the interface and the cell walls, the liquid surface was slightly concave at its edge and nearly flat at its center, where particles progressively accumulated by gravity (Fig. 1b and S1). Initially disordered, the particle assembly started to crystallize after about 16 min, *i.e.*, when a sufficient number of particles accumulated at the center. This concentration-dependent crystallization was due to the collective deformation of the interface by the accumulated particles,

which gave rise to an additional deformation that favored particle self-confinement at the interface center. This self-amplifying mechanism, also called "collective sinking",[39] resulted in a long-range attractive potential between repulsive anionic particles, thus inducing their crystallization.[17] In this work, we fixed the particle concentration (C_p = 0.05 mg·mL^{-1}, unless otherwise indicated) so that polycrystalline assemblies with a typical diameter of 0.57 ± 0.05 mm were obtained after about 70 min (Fig. 1b). Under ambient light conditions, these assemblies were stable and displayed a close-packed hexagonal order (Fig. 1c, I). To homogenously irradiate the particle assembly, a 4 mm light spot (λ = 440 nm) of controlled intensity was applied. Upon light exposure, the absorbing particles dissipated heat to the surrounding liquid, leading to perturbation of the equilibrium state and allowing us to remotely control the particles assembly, from modification of the lattice interparticle spacing (*IPS*) (Fig. 1c, II), to full melting of the 2D assembly (Fig. 2) depending on light intensity (*I*) and irradiation time.

Precise control over the inter-particle distance in 2D crystals. We first analyzed the response of the 2D ordered structures to a moderate light irradiation intensity ($I \leq 28.9$ W·m^{-2}). We applied cycles of 20 s light off/on and measured the *IPS* averaged over a sample area containing around 400 particles, as a function of time (Fig. 1d). While the original hexagonal arrangement of the particles under such conditions was not perturbed, an immediate and repeatable change in *IPS* was observed after each switch. By varying the light intensity, we could tune the shift in *IPS* from around 10 nm to around 130 nm when *I* increased from 2.7 W·m^{-2} (Fig. S2) to 28.9 W·m^{-2} (Fig. 1d, light-green points). For instance, irradiation at 11 W·m^{-2} resulted in an increase of *IPS* by approximately 40 nm in less than 4 s, followed by a steep decrease to the initial value as soon as light was removed (Fig. 1d, dark-blue points, Movie S1). This shift in lattice periodicity was robustly obtained for at least 5 consecutive cycles as well as in the case of longer period of irradiation (4 min, Fig. S2). For higher light intensities, the light-induced *IPS* change was larger but 20 s without stimulation were not enough to allow complete relaxation of the crystal structure to the initial *IPS* value, which thus slightly increased upon successive irradiation cycles. We thus demonstrated that such system of colloidal particles at the air/water interface advantageously converted light into thermal energy allowing to dynamically control the interparticle distance in ordered structures. For the experimental conditions used, the maximal increase of *IPS* we could reach without losing the ordered lattice structure was around 130 nm (I = 28.9 W·m^{-2}). Below this threshold, the conversion of absorbed light into thermal energy caused an expansion of the crystal, thus modifying the *IPS* and decreasing the particle density, while the long-range attraction due to collective sinking[39] was strong enough to keep the particle assembly in a crystalline state.

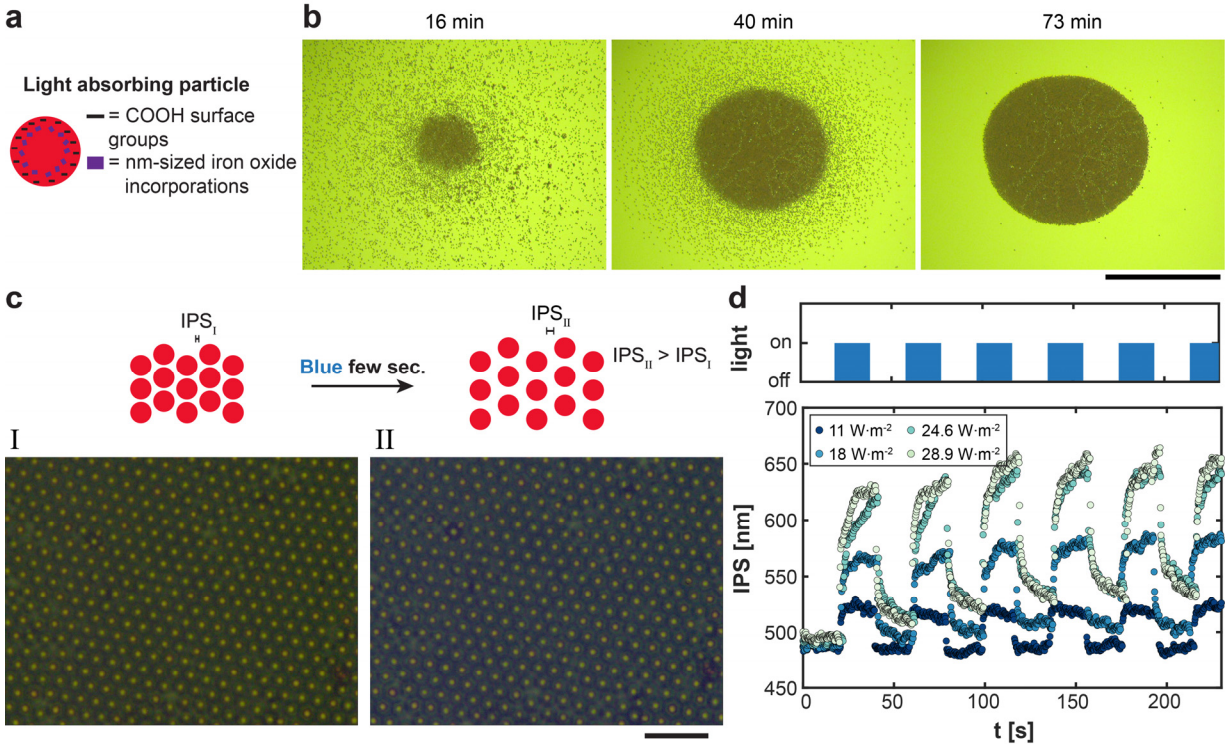

Figure 1. Dynamic photothermal control of interparticle spacing (*IPS*) in a two-dimensional colloidal crystal. a) Sketch of the light-absorbing particles (D_p = 4.5 µm) used in this study and containing iron oxide inclusions (for light absorption) and functionalized with carboxyl surface groups (anionic surface charge). b) Brightfield transmission microscopy images of the particles shown in a) at a concentration C_p = 0.05 mg·mL^{-1}, adsorbed at the air/water interface using the "flipping method" with DTAB cationic surfactant (C_s = 1 µM), and accumulating over time at the center of the concave interface to form a 2D crystal. Time starts right after the second flipping step. Scale bar: 500 µm. c) Sketch of the variation in *IPS* upon few seconds of light irradiation (top) and brightfield transmission microscopy images (bottom) of the center of the colloidal crystal at the air/water interface before (I, left) and after (II, right) 20 s of blue light irradiation (I = 24.6 W·m^{-2}). Scale bar: 20 µm. d) Scheme of light stimulation profile (top) and averaged *IPS* response in the crystal structure (bottom) to 20 s on/off light cycles with increasing intensities (dark to light symbols).

Light-induced melting and re-crystallization. When the 2D crystals were irradiated for a longer time and at higher light intensities, the increase in *IPS* was accompanied by a dramatic change in the organization of the whole particle assembly (Fig. 2). In such case, we observed a significant expansion accompanied by the complete melting of the crystalline structures (Fig. 2a, I) upon few minutes of irradiation (Fig. 2a, II), probably due to the decrease of the long-range attractive potential between particles through collective sinking. Interestingly, this process was reversible as it was followed by a re-crystallization of the particle assembly when the stimulus was removed (Fig. 2a, III and Movie S2). We calculated the radial distribution functions (RDF) to gain quantitative information on the order-to-disorder and subsequent disorder-to-order transitions. Prior to irradiation, the RDF showed well-defined peaks typical of hexagonal packing up to

distances (r) normalized with respect to the particle diameter (D_p) of $r/D_p = 6$ and positive peaks up to $r/D_p = 10$ (Fig. 2a, I). Upon light irradiation, the particles reached a disordered state within 4 min of light excitation, for $C_p = 0.05$ mg·mL^{-1} and $I = 39.5$ W·m^{-2}, with a liquid-like RDF displaying no structural order (Fig. 2a II). Due to the collective sinking mechanism, the long-range attractive potential between interfacial particles decreases with their concentration; therefore, in the case of a lower number of adsorbed particles, complete melting was obtained in a much shorter time (around 70 s for $C_p = 0.01$ mg·mL^{-1}, Fig. S3). These light-induced melting transitions were due to the particle-mediated conversion of light into thermal energy as 2D ordered arrays of polystyrene particles transparent to visible light were insensitive to irradiation (Fig S4). Moreover, in the absence of irradiation, when the experiment was performed with light-absorbing particles at a higher but homogenous temperature over the whole interface (up to 37 °C, Fig. S5), the particle assembly remained crystalline showing that the generation of a temperature gradient between particles and the surrounding interface was necessary for the melting to occur. After removal of the stimulation, particles assembled back into crystals with a hexagonal lattice similar to the initial one (Fig. 2a III). Note that, in this latter state, we observed smaller crystal domains compared to the initial structure, and the corresponding RDF displayed less defined peaks for $r/D_p > 5$. This increase in polycrystallinity can be explained by considering a history-dependent crystallization process. Packing in state (I) was obtained by a slow collection of interfacial particles at the center of the cell due to gravity (Fig. 1a), leaving time for particles to organize in an ordered state in around 20 min. The crystal domains size progressively increased, up to a final structure reached in around 70 min, where the number of defects was minimal. Conversely, the structure in state (III) was reached starting from a densely disordered phase already containing all the particles in close proximity, thus generating frustrated states and making it difficult for the particles to rearrange and repair eventual errors during crystal formation.

For a quantitative study of the transition kinetics, we followed the evolution of the mid-range order by plotting the height h_2 of the second peak in the RDFs as a function of time (Fig. 2b). From a value of $h_2 = 3$ in the initial ordered structure, the height of this peak progressively decreased as the structure became amorphous under illumination. This kinetics could be controlled by the applied light intensity. At $I = 39.5$ W·m^{-2}, melting was obtained in less than 200 s and with a complete loss of periodicity ($h_2 \simeq 1$). Instead, for lower intensities the equilibrium was reached in a longer timescale: 400 s and 500 s for $I =$ 33.6 W·m^{-2} and 26.8 W·m^{-2} respectively, and the final arrangement still presented a short-range periodicity as suggested by the slightly higher final value of h_2 and remaining unresolved peaks in the RDFs (Fig. S6). Interestingly, the melting transition displayed a bi-exponential behavior captured by the fits in Fig. 2B, with a first characteristic time of ~ 5 s followed by a much longer one, ranging from 100 s to 150 s (Table S1). This second characteristic time, which represents the overall time needed to reach fully disordered state,

decreased with an increase in irradiation power and can be related to a diffusion-controlled melting mechanism that will be analyzed in the next section.

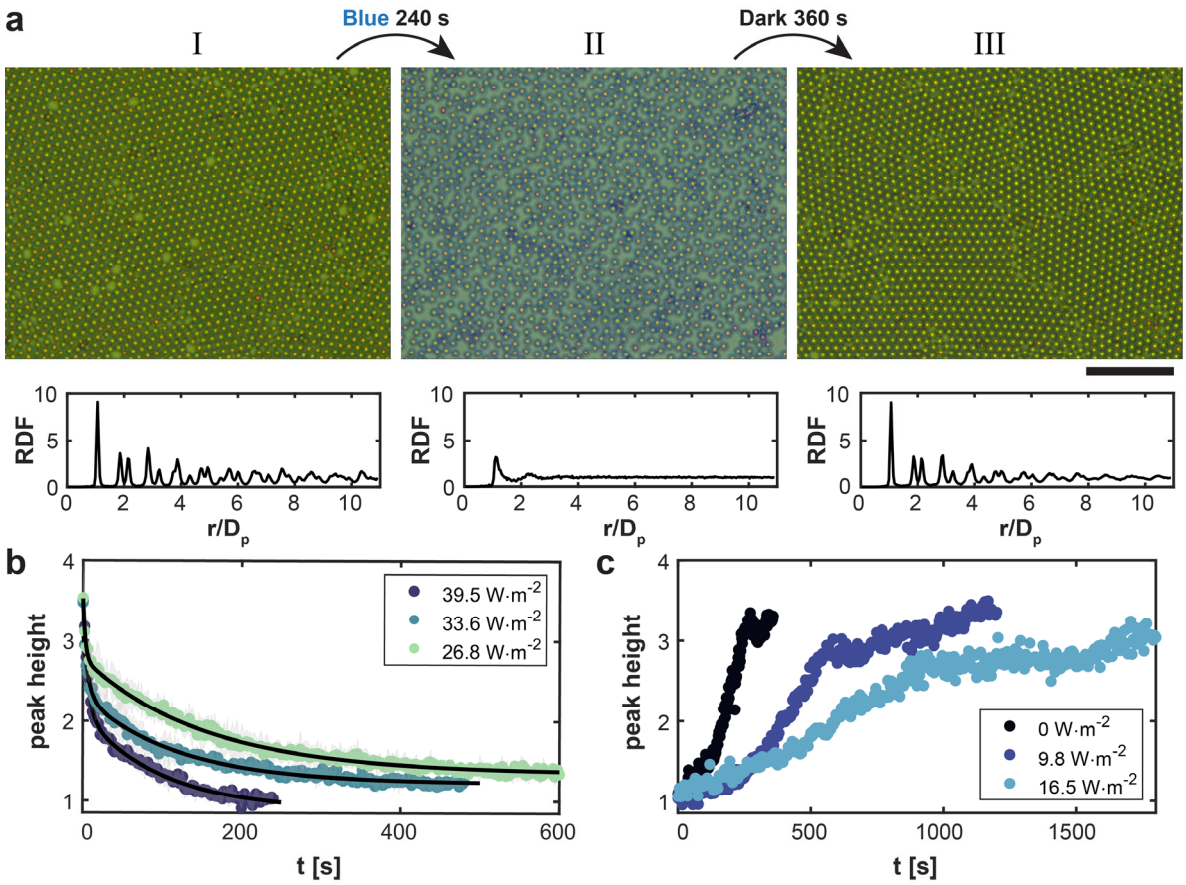

Figure 2. Light-controlled melting and re-crystallization of 2D colloidal assemblies. a) Brightfield transmission microscopy images and associated radial distributions functions (RDFs) of the center of the colloidal crystal at the air/water interface, at C_p = 0.05 mg·mL^{-1}, before (I, left), after 240 s of blue irradiation at I = 39.5 W·m^{-2} (II, middle), and after 360 s in ambient light condition (III, right). Scale bar: 50 µm. b) Kinetics of melting, quantified following the height of the second peak in the RDFs (h_2) as a function of time for constant light irradiation at different intensities. Symbols and shaded regions show mean values ± sd from three individual experiments. Solid lines are double-exponential fits (see parameters in Table S1). c) Kinetics of re-crystallization under different light intensities, after melting at I = 39.5 W·m^{-2} for 4 min.

We then focused on the subsequent disorder-to-order transition. All samples were first melted in the same conditions (I = 39.5 W·m^{-2} for 4 min) and then allowed to re-crystallize under different light intensities. Three conditions were performed successively on the same sample to rule out any interference, in the kinetics or in the final state, which could be due to the presence of specific imperfections (Fig. 2c). In the

dark (I = 0 W·m^{-2}, black dots), the final state was reached in around 300 s. The sample was melted a second time and left under constant light irradiation at 9.8 W·m^{-2} (blue dots, Fig. 2c), leading to a slower kinetics of re-crystallization ($t_{crystal}$ = 1100 s) but a similar ordered state in terms of number of defects and grain boundaries (Fig. S7). Finally, the sample was melted a third time and re-crystallized under I = 16.5 W·m^{-2}. A crystal structure, qualitatively similar to the two previous ones, was obtained in around 28 min (Fig. S7). Two additional experiments were performed on similar samples to externally control the process of re-crystallization after reaching the disordered phase (Fig. S8). After melting the crystals at I = 39.5 W·m^{-2} for 4 min, we progressively decreased in a continuous manner the light intensity until switching off the stimulus. The re-crystallization kinetics was following the decrease in light intensity, with a longer $t_{crystal}$ for the sample subjected to a slower rate of stimulus removal. Instead, the final state was once again similar to those observed in the previous conditions. Overall, a comparable number of grain boundaries and defects could be identified, whether the crystal was obtained under dark conditions (Fig. 2a (III)), fixed light irradiation (Fig. S7) or continuous decrease of the light intensity (Fig. S8). These results show how light intensity allowed one to finely tune the kinetics of both melting and recrystallization of interfacial particles without affecting the crystallinity, which was mainly set by the inherent particle polydispersity.

Melting/re-crystallization mechanism from single particle analysis. To get a better insight into this light-induced phase transitions and to quantify the monolayer response, we used single-particle tracking from optical microscopy images to map the instant velocity field and compute particles diffusivity (Fig. 3). Particles continuously tracked during the whole melting or re-crystallization process are displayed in Fig. 3a-b. When light was turned on, we first observed a rapid and strong outward radial flow (up to 4 μm·s^{-1}) that could be attributed to a thermally-driven Marangoni stress at the interface (Fig. 3a, 1-2). This stress was caused by the difference of surface tension between the free water surface surrounding the particle assembly (higher surface tension) and the locally heated region occupied by particles where the water surface tension was thus decreased. The increase in temperature around such particles was expected to be of the order of a few degrees,[28] while the dependence of the water surface tension on temperature is typically in the range of 0.1 mN·m^{-1}·K^{-1}.[40] The resulting surface tension gradient $\Delta\gamma$ thus allowed the generation of sufficiently strong Marangoni flows (of velocities $V_{Ma} \sim \Delta\gamma/\mu$ for a free interface with fluid viscosity μ) to expand the particle assembly. This confirmed the necessity of exploiting a gradient rather than a homogenous increase of temperature (Fig. S5) to affect the organization of the particle assembly. After a few seconds, this initial expansion led to a more progressive increase in the interparticle distance, particles trajectories became less directional and velocity decreased (Fig. 3a, 3-4), suggesting a diffusion-driven process due to the increase in temperature and in the free space available for particle motion. Similarly, the

re-crystallization started with a strong inward flow immediately after switching off light, and particle packing was then slowly obtained by diffusion and collective sinking (Fig. 3b).

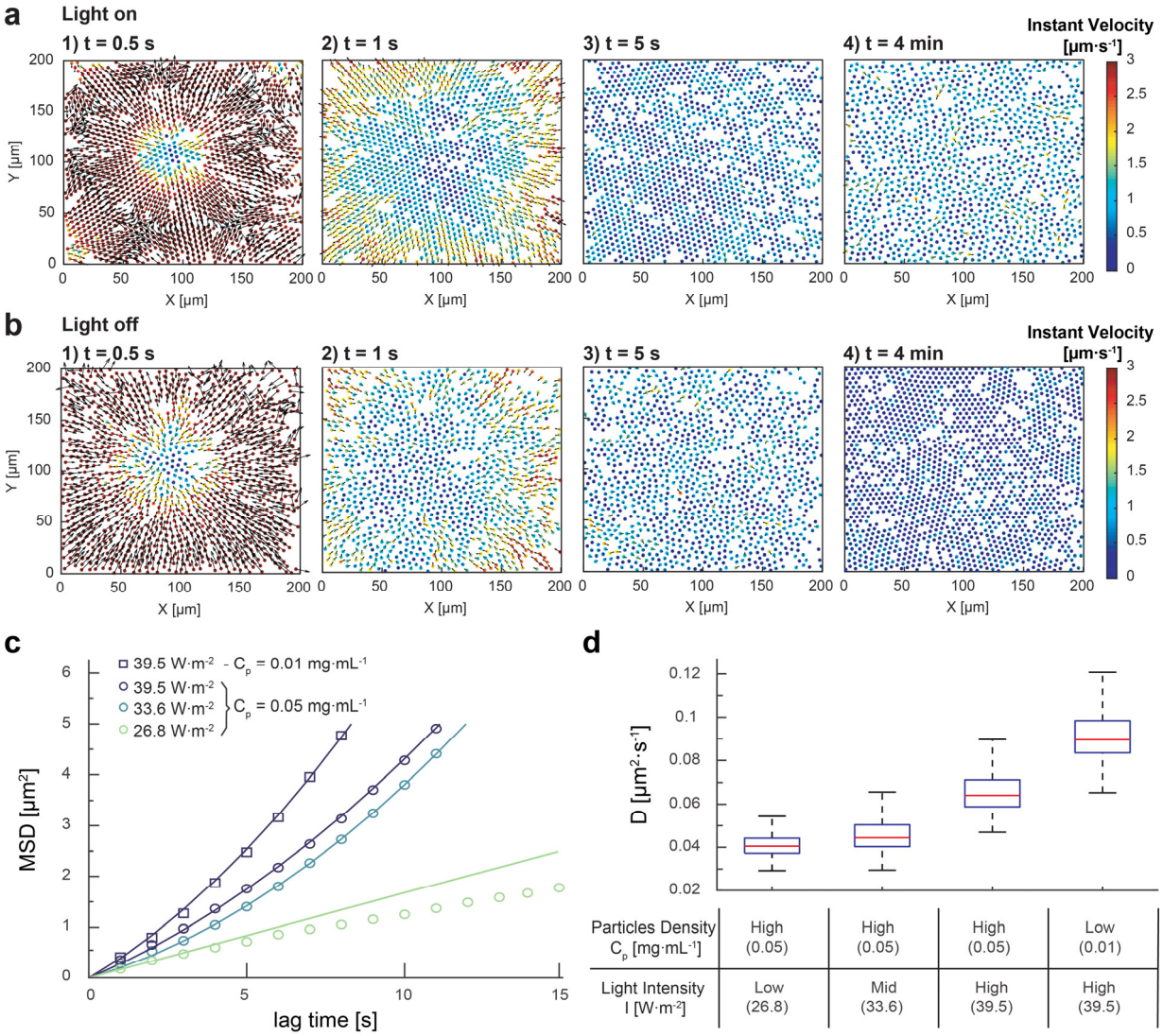

Figure 3. Single particle tracking shows that thermally-driven Marangoni stress and free diffusion are responsible for the melting mechanism. a) Instantaneous velocity field of particles during the light-driven melting process (I = 39.5 W·m^{-2}, C_p = 0.05 mg/mL) at different time (t) after switching on the light stimulus. Only particles with fully reconstructed trajectories where kept for analysis, leaving apparent voids in the structure. b) Instantaneous velocity field of particles during the re-crystallization process at different time (t) after switching off the light stimulation. c) Average mean square displacement (MSD, symbols) of particles in the melted state for different conditions of light intensity and particle concentrations. MSD were fitted by a biased Brownian motion (lines): $MSD = 4 \cdot D \cdot t + (V \cdot t)^2$ where D and V are the diffusion coefficient and the drift velocity, respectively. d) Box plot of the diffusion coefficients (D) obtained from data fit of single particle MSD as in c, for increasing light intensities and decreasing particle concentration (red line: median, blue box: 1st and 3rd quartiles, extremity bars: extreme points).

For a more quantitative insight, we imaged particles at higher magnification, reconstructed their trajectories and computed their mean square displacement (*MSD*) as a function of the lag time for single trajectories to extract the median *MSD* for the different intensities and concentrations (Fig. 3c). We performed the analysis in melted samples when an apparent steady state was reached. First we fitted each single trajectory (*c.a.* 700 trajectories for each condition) with a generalized diffusion model, $MSD = D_G \cdot t^{\alpha}$, where D_G is the so-called generalized diffusion coefficient and α an exponent characterizing the type of diffusive motion (Figs. S9 and S10). For low light intensity (I = 26.8 W·m^{-2}), particles mainly experienced a subdiffusive motion (α = 0.76 ± 0.1), due to an insufficient unpacking in the melted state. Conversely, at higher intensities particles motion was typically superdiffusive (α > 1), with α = 1.50 ± 0.06 (I = 33.6 W·m^{-2}, C_p = 0,05 mg·mL^{-1}), α = 1.36 ± 0.07 (I = 39.5 W·m^{-2}, C_p = 0,05 mg·mL^{-1}) and α = 1.41 ± 0.06 (I = 39.5 W·m^{-2}, C_p = 0,01 mg·mL^{-1}). This superdiffusive behavior could be explained by the presence of additional modes of transport of particles in the melted state, probably due to hydrodynamic interactions and large scale rearrangements in the structure (Fig. S9, right). To extract the purely Brownian contribution, MSD curves were then fitted using a biased Brownian model ($MSD = 4 \cdot D \cdot t + (V \cdot t)^2$), with diffusion coefficient D (Fig. 3d) and a drift velocity V (Fig. S11) accounting for the additional flows. For the trajectories at the lowest light intensity (subdiffusive behavior), data were fitted on a shorter timescale to better estimate the diffusion coefficient. We found an increase in Brownian motion with increasing light intensity (Fig. 3d), which confirmed a general effect of heat dissipation due to light adsorption by the particles. Notably, we found that this measured diffusion coefficient in the melted state correlated with the inverse of the long characteristic time observed in Fig. 2b, leading to a constant characteristic diffusive length $L_{Diff} \approx 4.9$ µm (Fig. S12), which is of the same order of the particle size. This shows that, after a fast Marangoni-driven expansion, the transition kinetics from crystalline to melted state was limited by the Brownian diffusion of individual particles in the assembly, which in turn was directly tuned by light intensity. Diffusion was also increased when lowering particles concentration (0.01 instead of 0.05 mg·mL^{-1}, Fig. 3d right), suggesting a trade-off between attraction potential caused by collective sinking and particle diffusion in a crowded environment.

Local melting and dynamic structures. Finally, we investigated the versatility of our approach to control the organization of 2D colloidal assemblies. First, we evaluated the possibility of creating melted/crystalline hybrid patterns by applying local irradiation. To this end, we used a custom-built set-up where a light beam (*c.a.* 100 µm diameter at the focal plane, λ = 410 nm, $I = 1.4 \cdot 10^3$ W·m^{-2}) was coupled with an inverted microscope to track the particle positions.[38] Precise spatial melting of the colloidal assembly was achieved by irradiating a large crystal structure (C_p = 0.1 mg·mL^{-1}, colloidal assembly diameter ≈ 0.8 mm, Fig. 4a,

Movie S3). In this case, we observed a rapid (< 2 s) and highly localized disassembly at the light spot, with only minor rearrangements of the surrounding crystalline structure. When the light spot was moved, the melted zone re-crystallized in a few seconds, while a new region under light rapidly disassembled. This was possible because, for this crystal dimension, the thermally induced perturbation was not sufficient to counteract, on a large scale, the overall collective sinking, due to the large number of particles at the air/water interface. As a result, we could achieve precise guidance and transport of a locally melted zone in a large 2D crystal thus capable of self-healing. When local irradiation was applied on a much smaller crystal structure (C_p = 0.05 mg·mL^{-1}, crystal diameter ≈ 0.26 mm, Fig. S13 and Movie S4), a rapid melting (< 2 s) of the colloidal assembly was also obtained but the melted zone was larger than the light spot size. This was expected due to the small crystal dimension, and consequent packing forces experienced by the particles, with respect to the spot size. Complete recovery of the ordered structure was possible after light removal (Fig. S13). A different behavior was evidenced when a small crystal structure was locally irradiated for a continuous period of time. Interestingly, continuous irradiation at the edge of such small crystal patches allowed to reach a steady-state crystallization coupled to a permanent flow of particles from the melted zone to the crystallized central area (Fig. 4b, Movie S5). Light stimulation triggered the local melting of the crystal and the heated particles were pushed away by radial Marangoni flows. Due to the geometrical constraints at the curved air/water interface, particles remained trapped to the proximity of the structure, circumnavigated the crystal and re-assembled in the non-irradiated zone (Fig. 4b, right). This resulted in a motion of particles in the crystallin domain toward the illuminated side, where melting occurs, with a quasi-steady state crystalline structure in the middle (Fig. S14). This system is thus a new example of living crystallization in a 2D colloidal system. Here, it originates from the coupling between interface curvature and local disassembly and also differs with what has been reported with phoretic Janus colloids[26] for the fact that particles, in our case, melt and recrystallize within the same cluster. To gain in multifunctionality, we took advantage of the magnetic properties of the embedded iron oxide inclusions in our particles to control transitions between different 2D structures upon combined light and magnetic actuation. In a representative experiment (Fig. 4c), a 2D crystal at the air/water interface was first irradiated with blue light (I = 39.5 W·m^{-2}, 4 min) causing melting of the hexagonal array. Approaching a small permanent magnet to the melted structure allows ordering of the magnetic colloids into parallel chains in ~ 2 s timescale. Conversion back to the amorphous state follows removal of the magnetic stimulus. Such amorphous state rearranges into a 2D crystal if left in the absence of light irradiation. Transitions between 2D crystals, amorphous structures and parallel chains were all reversible, with light irradiation causing full melting of any initial structure.

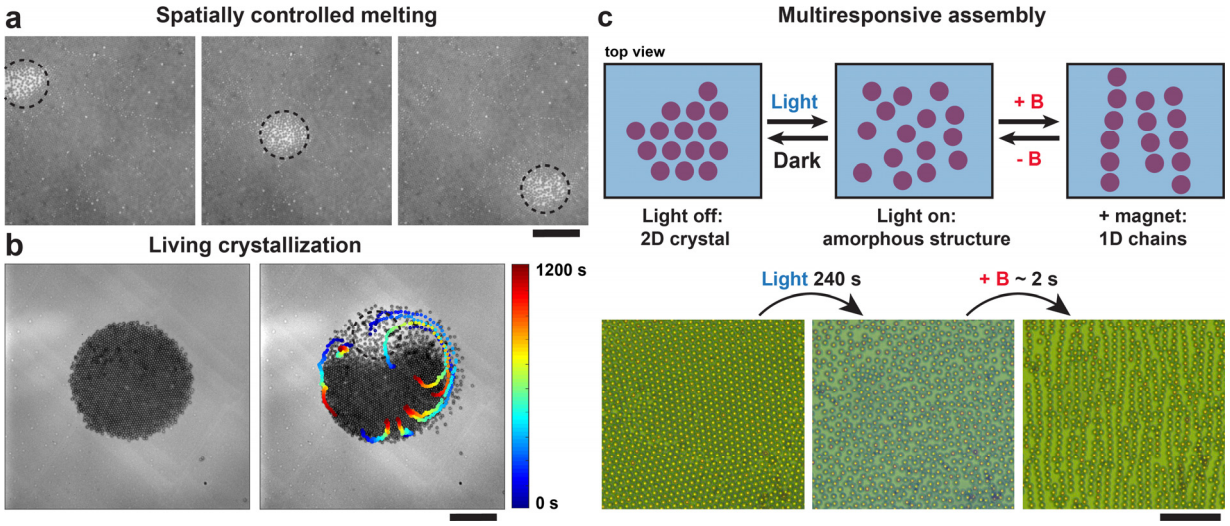

Figure 4. Versatility over the structural organization of 2D colloidal assemblies under light and/or magnetic stimulation. a) Brightfield reflection microscopy images of a colloidal crystal at the air/water interface (C_p = 0.1 mg·mL^{-1}), subjected to a focused light irradiation moved at different positions (dotted circles, λ = 410 nm, $I = 1.4 \cdot 10^3$ W·m^{-2}). Time between the images: 20 s (see Movie S3). Scale bar : 100 µm. b) "Living" colloidal crystal under continuous focused light irradiation (C_p = 0.05 mg·mL^{-1}, see Movie S5). Initial state at ambient light condition (left) and superimposition of the image of the colloidal crystal after 20 min of light irradiation focused in the dotted circle including the tracking of eight particles trajectories from the beginning until the end of the light irradiation (right). Scale bar : 100 µm. c) Coupling of magnetic and light control. Sketch of the different colloidal arrangements and of the stimuli required to reach them (top) and brightfield transmission microscopy images of a colloidal monolayer (bottom) before light irradiation (I = 39.5 W·m^{-2}, 4 min, left), after blue light irradiation (middle), and immediately after approaching a permanent magnet parallel to the liquid interface (right). Scale bar: 50 µm.

Conclusions

In summary, we showed how light-absorbing microparticles adsorbed at an air/water interface can be used as an efficient platform for achieving precise spatial and temporal control over the structural organization of 2D colloidal assemblies. We used minute amounts of a cationic surfactant to induce the adsorption of anionic particles at the air/water interface. The combination of short-range electrostatic repulsion between the particles and long-range attraction by collective sinking[17,18] led to their self-assembly into 2D polycrystalline close-packed structures, which were stable in the absence of light. Under visible light irradiation, particles were absorbing light and dissipating heat locally creating a Marangoni-induced expansion of the assembly, counteracting the local confinement of particles in the center of the interface they deformed due to the collective sinking mechanism.[39] With short pulses of light irradiation at low intensity, the assembly remained crystalline and the photostimulation enabled a precise control of the

interparticle spacing (*IPS*), with an increase of the *IPS* from 10 nm to 130 nm as function of the light intensity. Higher-irradiation intensities increased the assembly expansion and allowed for a progressive melting of the structures, with a kinetics limited by the diffusion of individual particles previously confined in the close-packed assembly. As a consequence, the kinetics of the melting could be tuned by changing the light intensity through the thermal dependence of the particle diffusion coefficient. In all cases, removing the light stimulation resulted in the recrystallization of the particle assembly, dictated by the collective sinking toward the center of the assembly. We also explored the versatility of our system to respond to patterned light irradiation, and to a combination of light and magnetic actuation. This allowed us to dynamically guide and transport a local melted zone in a large colloidal assembly remaining crystalline in the non-irradiated area. With a smaller assembly, the localized melting of the crystal coupled to the interface curvature resulted an unusual, dynamic steady-state of triggered dissolution under the light spot and collective re-organization in the non-irradiated periphery of the crystal. This led to the formation of a new kind of living crystal made of self-fed particles. Finally, coupling with magnetic control allowed us to switch between 2D crystals, amorphous assemblies and 1D chains in a fully reversible fashion.

Overall, these results open the way to a novel, simple yet powerful, mechanism to dynamically arrange monolayers of particles, where fine tuning of interparticle spacing and/or melting/crystallization transitions can be achieved with high spatio-temporal control, in a fast and reliable manner. This creates an ideal platform not only to generate addressable 2D soft materials but also to study interfacial organization and 2D colloidal phase transitions. Besides the achievements made possible by this photocontrol approach, an interesting feature lies in its inherent mechanism. Here, contrary to already explored approaches, the energy transduction from the light stimulus to the crystal response is not based on photochromism nor light-dependent particle-particle interactions, which both require specific interface engineering, but on a more generic principle of heat dissipation through visible light absorption by non-transparent particles.[28,33,34] This allows to better understand the role of temperature in ordered colloidal assemblies as well as makes this principle particularly straightforward to be implemented in real-world devices based on colloidal assemblies at liquid interfaces.[41]

Supporting Information. Materials and methods; supplementary figures S1-S14; table S1; movies S1-S5 and their legends.

References

1. Vogel, N., Retsch, M., Fustin, C.-A., del Campo, A. & Jonas, U. Advances in Colloidal Assembly: The Design of Structure and Hierarchy in Two and Three Dimensions. *Chem. Rev.* **115**, 6265–6311 (2015).
2. Xia, Y., Gates, B., Yin, Y. & Lu, Y. Monodispersed Colloidal Spheres: Old Materials with New Applications. *Adv. Mater.* **12**, 693–713 (2000).
3. McGorty, R., Fung, J., Kaz, D. & Manoharan, V. N. Colloidal self-assembly at an interface. *Mater. Today* **13**, 34–42 (2010).
4. Grzelczak, M., Vermant, J., Furst, E. M. & Liz-Marzan, L. M. Directed Self-Assembly of Nanoparticles. *ACS Nano* **4**, 3591–3605 (2010).
5. Tran, L. & Haase, M. F. Templating Interfacial Nanoparticle Assemblies via in Situ Techniques. *Langmuir* **35**, 8584–8602 (2019).
6. Isa, L. *et al.* Particle Lithography from Colloidal Self-Assembly at Liquid−Liquid Interfaces. *ACS Nano* **4**, 5665–5670 (2010).
7. Fang, P.-P. *et al.* Conductive Gold Nanoparticle Mirrors at Liquid/Liquid Interfaces. *ACS Nano* **7**, 9241–9248 (2013).
8. Turek, V. A. *et al.* Plasmonic Ruler at the Liquid–Liquid Interface. *ACS Nano* **6**, 7789–7799 (2012).
9. Vogel, N., de Viguerie, L., Jonas, U., Weiss, C. K. & Landfester, K. Wafer-Scale Fabrication of Ordered Binary Colloidal Monolayers with Adjustable Stoichiometries. *Adv. Funct. Mater.* **21**, 3064–3073 (2011).
10. Edel, J. B., Kornyshev, A. A. & Urbakh, M. Self-Assembly of Nanoparticle Arrays for Use as Mirrors, Sensors, and Antennas. *ACS Nano* **7**, 9526–9532 (2013).
11. Fernández-Rodríguez, M. Á. *et al.* Tunable 2D binary colloidal alloys for soft nanotemplating. *Nanoscale* **10**, 22189–22195 (2018).
12. Grillo, F., Fernandez-Rodriguez, M. A., Antonopoulou, M.-N., Gerber, D. & Isa, L. Self-templating assembly of soft microparticles into complex tessellations. *Nature* **582**, 219–224 (2020).
13. Srivastava, S., Nykypanchuk, D., Fukuto, M. & Gang, O. Tunable Nanoparticle Arrays at Charged Interfaces. *ACS Nano* **8**, 9857–9866 (2014).
14. Truzzolillo, D., Sharaf, H., Jonas, U., Loppinet, B. & Vlassopoulos, D. Tuning the Structure and Rheology of Polystyrene Particles at the Air–Water Interface by Varying the pH. *Langmuir* **32**, 6956–6966 (2016).
15. Reynaert, S., Moldenaers, P. & Vermant, J. Control over Colloidal Aggregation in Monolayers of Latex Particles at the Oil−Water Interface. *Langmuir* **22**, 4936–4945 (2006).
16. Park, B. J. *et al.* Direct Measurements of the Effects of Salt and Surfactant on Interaction Forces between Colloidal Particles at Water−Oil Interfaces. *Langmuir* **24**, 1686–1694 (2008).
17. Anyfantakis, M. *et al.* Adsorption and Crystallization of Particles at the Air–Water Interface Induced by Minute Amounts of Surfactant. *Langmuir* **34**, 15526–15536 (2018).
18. Vialetto, J., Rudiuk, S., Morel, M. & Baigl, D. From bulk crystallization of inorganic nanoparticles at the air/water interface: tunable organization and intense structural colors. *Nanoscale* **12**, 6279–6284 (2020).
19. Tao, A., Sinsermsuksakul, P. & Yang, P. Tunable plasmonic lattices of silver nanocrystals. *Nat. Nanotechnol.* **2**, 435–440 (2007).
20. Aveyard, R., Clint, J. H., Nees, D. & Paunov, V. N. Compression and Structure of Monolayers of Charged Latex Particles at Air/Water and Octane/Water Interfaces. *Langmuir* **16**, 1969–1979 (2000).
21. Rey, M., Law, A. D., Buzza, D. M. A. & Vogel, N. Anisotropic Self-Assembly from Isotropic Colloidal Building Blocks. *J. Am. Chem. Soc.* **139**, 17464–17473 (2017).
22. Klajn, R., Bishop, K. J. M. & Grzybowski, B. a. Light-controlled self-assembly of reversible and irreversible nanoparticle suprastructures. *Proc. Natl. Acad. Sci.* **104**, 10305–10309 (2007).
23. Kundu, P. K. *et al.* Light-controlled self-assembly of non-photoresponsive nanoparticles. *Nat. Chem.* **7**, 646–652 (2015).

24. Varanakkottu, S. N., Anyfantakis, M., Morel, M., Rudiuk, S. & Baigl, D. Light-Directed Particle Patterning by Evaporative Optical Marangoni Assembly. *Nano Lett.* **16**, 644–650 (2016).
25. Anyfantakis, M., Varanakkottu, S. N., Rudiuk, S., Morel, M. & Baigl, D. Evaporative Optical Marangoni Assembly: Tailoring the Three-Dimensional Morphology of Individual Deposits of Nanoparticles from Sessile Drops. *ACS Appl. Mater. Interfaces* **9**, 37435–37445 (2017).
26. Palacci, J., Sacanna, S., Steinberg, A. P., Pine, D. J. & Chaikin, P. M. Living Crystals of Light-Activated Colloidal Surfers. *Science* **339**, 936–940 (2013).
27. Singh, D. P., Choudhury, U., Fischer, P. & Mark, A. G. Non-Equilibrium Assembly of Light-Activated Colloidal Mixtures. *Adv. Mater.* **29**, 1701328 (2017).
28. Schmidt, F., Liebchen, B., Löwen, H. & Volpe, G. Light-controlled assembly of active colloidal molecules. *J. Chem. Phys.* **150**, 094905 (2019).
29. Zaidouny, L., Bohlein, T., Roth, R. & Bechinger, C. Light-induced phase transitions of colloidal monolayers with crystalline order. *Soft Matter* **9**, 9230 (2013).
30. Cash, C. E. *et al.* Local Melting Attracts Grain Boundaries in Colloidal Polycrystals. *Phys. Rev. Lett.* **120**, 018002 (2018).
31. Girot, A. *et al.* Motion of Optically Heated Spheres at the Water–Air Interface. *Langmuir* **32**, 2687–2697 (2016).
32. Varanakkottu, S. N. *et al.* Particle Manipulation Based on Optically Controlled Free Surface Hydrodynamics. *Angew. Chemie Int. Ed.* **52**, 7291–7295 (2013).
33. Dietrich, K., Jaensson, N., Buttinoni, I., Volpe, G. & Isa, L. Microscale Marangoni Surfers. *Phys. Rev. Lett.* **125**, 098001 (2020).
34. Maggi, C., Saglimbeni, F., Dipalo, M., De Angelis, F. & Di Leonardo, R. Micromotors with asymmetric shape that efficiently convert light into work by thermocapillary effects. *Nat. Commun.* **6**, 7855 (2015).
35. Chevallier, E. *et al.* Pumping-out photo-surfactants from an air–water interface using light. *Soft Matter* **7**, 7866 (2011).
36. Caciagli, A., Joshi, D., Kotar, J. & Eiser, E. Optical trapping of colloids at a liquid-liquid interface. *ArXiv* (2017).
37. Caciagli, A., Singh, R., Joshi, D., Adhikari, R. & Eiser, E. Controlled Optofluidic Crystallization of Colloids Tethered at Interfaces. *Phys. Rev. Lett.* **125**, 068001 (2020).
38. Vialetto, J., Anyfantakis, M., Rudiuk, S., Morel, M. & Baigl, D. Photoswitchable Dissipative Two-Dimensional Colloidal Crystals. *Angew. Chemie Int. Ed.* **58**, 9145–9149 (2019).
39. Lee, D.-G., Cicuta, P. & Vella, D. Self-assembly of repulsive interfacial particles via collective sinking. *Soft Matter* **13**, 212–221 (2017).
40. Vargaftik, N. B., Volkov, B. N. & Voljak, L. D. International Tables of the Surface Tension of Water. *J. Phys. Chem. Ref. Data* **12**, 817–820 (1983).
41. Montelongo, Y. *et al.* Electrotunable nanoplasmonic liquid mirror. *Nat. Mater.* **16**, 1127–1135 (2017).

Acknowledgements

We thank Thomas Bickel (University of Bordeaux) for insightful discussion. This work was supported by European Research Council (ERC) (European Community's Seventh Framework Programme (FP7/2007–2013)/ERC Grant Agreement No. 258782) and the Labex IPGG (ANR-10- LABX-31).

Competing interests

The authors declare no competing financial interest.

Graphical table of contents